Received February 17, 2021, accepted February 22, 2021, date of publication February 24, 2021, date of current version March 5, 2021.

Digital Object Identifier 10.1109/ACCESS.2021.3062299

Engineering Photonic Transmission Inside Brain Nerve Fibers

AMIR MAGHOUL[1], ALI KHALEGHI[1,2], AND ILANGKO BALASINGHAM[1,2]
[1]Department of Electronic Systems, Norwegian University of Science and Technology, 7491 Trondheim, Norway
[2]Intervention Center, Oslo University Hospital, 0027 Oslo, Norway

Corresponding author: Amir Maghoul (amir.maghoul@ntnu.no)

This work was supported by the European Research Consortium for Informatics and Mathematics (ERCIM), and Research Council of Norway funded project CIRCLE, under Grant 287112.

ABSTRACT Electrical signaling is known as the means for inter-cellular connectivity among neural cells. However, there are some indications that optical phenomena can occur in the neuronal cells based on biochemical processes in intra-or extracellular reactions. Also, external optical signals can be used to manipulate engineered neural cells for performing key functions. Motivated by these, this paper establishes a framework on photon transmission inside nerve fiber using optical properties of the nerve tissues to study photonic signaling. We use the same framework to analyze and propose mitigation using nanoparticles for demyelinated nerve channels- a potential cause for certain brain disorders like Alzheimer's disease. Our study assumes photons are available. The proposed framework for photonic signaling across nerve fibers uses an analytical model of a nerve fiber's segment that consists of physical factors, including size, Ranvier node presence, and interconnected segments. The demyelination effect on the nerve channel is evaluated by numerical electromagnetic computations. On this basis, photonic transmittance of a defected nerve segment is calculated, while demyelination takes place in different locations, lengths, and depths across the nerve segment. To repair the demyelination and enhance the transmittance of the demyelinated axon, we have performed analysis on nanoparticles such as silicon and silica quantum dots, gold nanoparticles, and gold/silica core-shell nanoparticles. Our computational models show that nanoparticles' presence improves the optical properties of nerve configuration that indicate photons can be transmitted in the axonal routes of demyelinated channels.

INDEX TERMS Axon channel, core-shell nanoparticle, demyelinated axon, nanorod, photonic transmission, transmittance, quantum dot.

I. INTRODUCTION

Employing electrical signals for medical applications, especially in the brain, is well understood. However, specialists still face challenges concerning signaling from tiny brain areas. Focusing on this and with the objective of designing effective treatments, new mechanisms have emerged. Optogenetics [1], [2], magnetogenetics [3], and radiogenetics [4] are examples in which unique approaches allow access to deep areas of the brain, and cell level signaling is established using intrinsic features of the brain tissues. Besides, from a physiological phenomena point of view [5], all living cells of organisms have also the potential to emit natural photons due to chemical and physiological interactions [6]–[8], although those are very weak; however, scientists are engaging in a broad range of studies [9]–[13] to develop new techniques such as chemo brain for photon release with the aim of neuronal signaling. It has proved that neurons contribute most to photon generation in the body [14] and enable continuous production of biophotons [15]–[17]. The intensity of biophoton emissions correlates with some neural activities, such as neuronal membrane depolarization and stimulation of ions such as Ca^{2+} and K^{+} [18], [19]. Biophotons primarily stem from the bioluminescent radical and non-radical reactions of reactive oxygen species and reactive nitrogen species. It has been proven that the oxidative metabolism of mitochondria functions as the main source of photon production inside a neuron [5], [19]–[21]. Despite the tiny structures of mitochondria and microtubules inside of axons, they enable optical signals to be conducted inside the nerve fiber and operate as waveguides [22]–[24].

Recent researches also indicate that the biochemical reactions, ion-transmembrane, energy level transitions of biomolecular activities in nerve cells can produce

The associate editor coordinating the review of this manuscript and approving it for publication was Sukhdev Roy.

biophotons [25], [26]. On the other hand, some neuro-optical manipulations [27] in which light interacts with nerve cells can produce a photonic current inside the nerve cell to operate similar to the incidence of light from external sources to arrive in the nerve fibers [28]. Afterward, photon cell-cell transport can be carried out through axonal routes, which convey signals between nerve cells and transfer photons to adjacent cells. Indeed, axons count as a proper platform for photonic signaling due to having a suitable configuration in which many microtubules and mitochondria exist [21], [29], [30]. In general, all strategies employed in this area have aimed to access smaller regions, such as single cells and deep brain tissues for diagnosis, rehabilitation, and treatment. Although recent experimental results have been published about the dynamic of these interactions, however many topological challenges remain still unclear, ranging from the nanoscale. Hence, a precise understanding of the structural concepts underlying the interaction between photons and neurons seems to be pivotal for research in nanomedicine. To fill this gap, computational configurations and nanoscale modeling are also employed to open relevant approaches and present initiative contributions, providing details that cannot be derived from experimental methods.

In this article, by assuming available photons in nerve cells apart from being natural or man-made, we first focus on a full-wave 3D computational model of the nerve fiber from an engineering viewpoint and numerically analyze photon transmission inside it. Recent findings [31] demonstrate that nerve fibers possess strong absorption in wavelengths close to 0.3μm. Hence, wavelengths ranging from 0.3μm to 0.9μm are chosen for our work. The effects of nerve fibers' physical factors, including size, length, Ranvier node dimensions, and second nerve segment connection, on the photonic signaling, are assessed for lossless and lossy models of the nerve segment. Besides, the influence of demyelination in positions and different sizes on nerve fiber is evaluated. Motivating by this, we propose a mechanism based on nanoparticles to repair photon transmission inside demyelinated nerve fibers that may affect modern techniques for treating brain disorders such as multiple sclerosis (MS) and Alzheimer's.

II. SYSTEM MODEL

From a morphological perspective, body tissues can be grouped into four standard biological categories: connective tissues, epithelial tissues, muscle tissues, and nervous tissues. The nervous system is primarily composed of neurons and glial cells. These cells construct the central nervous system and the peripheral nervous system of the brain [32]. The configuration of neurons, also called nerve cells, demonstrates a specific level of elasticity. The bio-physiological structure of a neuron comprises dendrites, a cell body, and a myelinated axon. Axons are responsible for transferring produced signals in a cell to the synapse terminal. The myelin sheath functions as an insulator. Some nodes cross the nerve fibers; ion channels are concentrated in these Ranvier nodes. The interaction between ions conducts signals within neurons

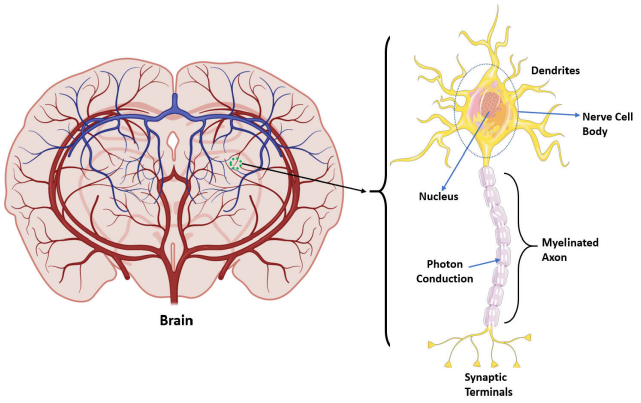

FIGURE 1. Schematic structure of Neuron in the brain.

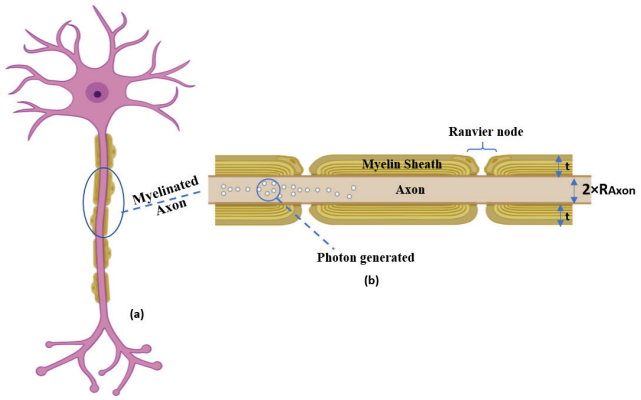

FIGURE 2. (a)Schematic of Single Neuron in the brain, (b) Myelinated Axon as a photonic Waveguide.

and is known as the action potential. Physical factors such as myelin thickness, which is correlated with the g-ratio [33], can influence the conduction of the nervous network [8], [31]. A schematic diagram of a neuron is illustrated in Fig.1.

Myelin thickness is correlated with the g-ratio, which is the ratio of the axon diameter over the nerve fiber diameter and is always smaller than 1. The Ranvier node is positioned between two segments of the myelinated axon. The size of the Ranvier node is about 1μm or 2μm [34]. At the end of each nerve segment before the Ranvier gap, which is non-compacted by myelin, the paranode is located. As demonstrated in Fig.2, the axon, myelin sheath, and Ranvier node comprise the main components of a nerve fiber.

In our work, a segment of a rat nerve fiber is modeled using real data obtained from measurements [8], [35], [36]. The length of the myelinated axon selected is about 27μm, and this value ranges to 82μm and 154μm. The g-ratio is 0.78, and this parameter varies between 0.6 and 0.8 for different nerve fibers. The axon radius is equivalent to 0.4μm in the model[31]. The myelin thickness is obtained through Equation (1):

$$\text{g-ratio} = 2 \times R_{Axon} / \left(2 \times R_{Axon} + 2 \times t_{myelin}\right). \quad (1)$$

The axon radius and myelin thickness are described by R_{Axon} and t_{Myelin}, respectively. The Ranvier gap is assumed to be 1μm as well.

III. RESULT

A. PHOTON TRANSITION IN NERVE FIBERS

Nerve fibers have the potential to function like optical fibers, allowing light to pass; however, there are many challenges to light transmission, such as absorbance and reflectance. From an optical viewpoint, the structure's refractive indices play an important role in light transmission inside the material. The presence of ions in the peripheral environment and inside the myelinated axon can form plasmon polaritons that influence the nerve segment's signaling. It has been proved that the number of ions and their interaction with the excitation signal create the surface plasmon polariton that makes propagation phenomena across the nerve fiber [37]–[40]. Extracting the precise model of nerve fiber underlying ions is led to face some complexities in the simulations due to lack of established experimental data regarding nerve fibers. Hence, in this work, the preference is to use the model proved in the valid literature [31], [35]. Accordingly, as shown in Fig. 3(a), the refractive index of the nerve fiber in this study is n = 1.38, 1.44, 1.34 for the axon, myelin sheath, and extracellular medium of neurons respectively [41]–[43]. The structure of the nerve fiber is initially hypothesized as lossless. The neuron's modeled configuration is implemented in the CST Microwave Studio for a 3D full-wave electromagnetic simulation. An engineering model of the nerve fiber based on established optical concepts is proposed. The current model is constructed using g-ratio = 0.78, axon radius = 0.4μm, and nerve fiber length = 27μm. In this model, photonic signal transmission through a single neuron is simulated. To extract structural coupling effects, the light emission is applied in the axon, and the light penetration is evaluated by placing an output port on the myelin and axon, as shown in Fig. 3(a). The efficiency of light coupling is calculated in Fig. 3(b). There is a downward trend in the spectral characteristic of the nerve fiber, which is rooted in the fact that the wavelength spectrum approaches the cut-off frequency of the nerve channel. More energy is coupled inside the myelin sheath for wavelength above 380nm, while the transmittance for wavelength below 380nm is considerable inside the axon channel. A broadening is also observed in spectral responses that result from the multi-path dispersion of a fiber [44], [45]. To demonstrate the electric field's profile inside the axonal zone, electric field distribution in two cross-sections: (A),(B) of nerve fiber at wavelengths 334nm, 399nm are illustrated in Fig.3(c). To better understand, 3D distributions of the electric fields in the structure at the aforementioned wavelengths are also shown in Fig.3(d).

Generally, the damaging myelin sheath is the main problem for signal discontinuity between neurons inside the brain that happens in different brain d μisorders. Besides, the greatest amount of biophotonic current related to neurons is supposed to transfer using mitochondria and microtubules inside axons [19], [22], [46]. Accordingly, the axon is presumed to be the central core of the nerve channel in which photonic current flows. As a part of the single nerve fiber, the paranode with a length of 500nm(Lp = 500nm) is also added to the

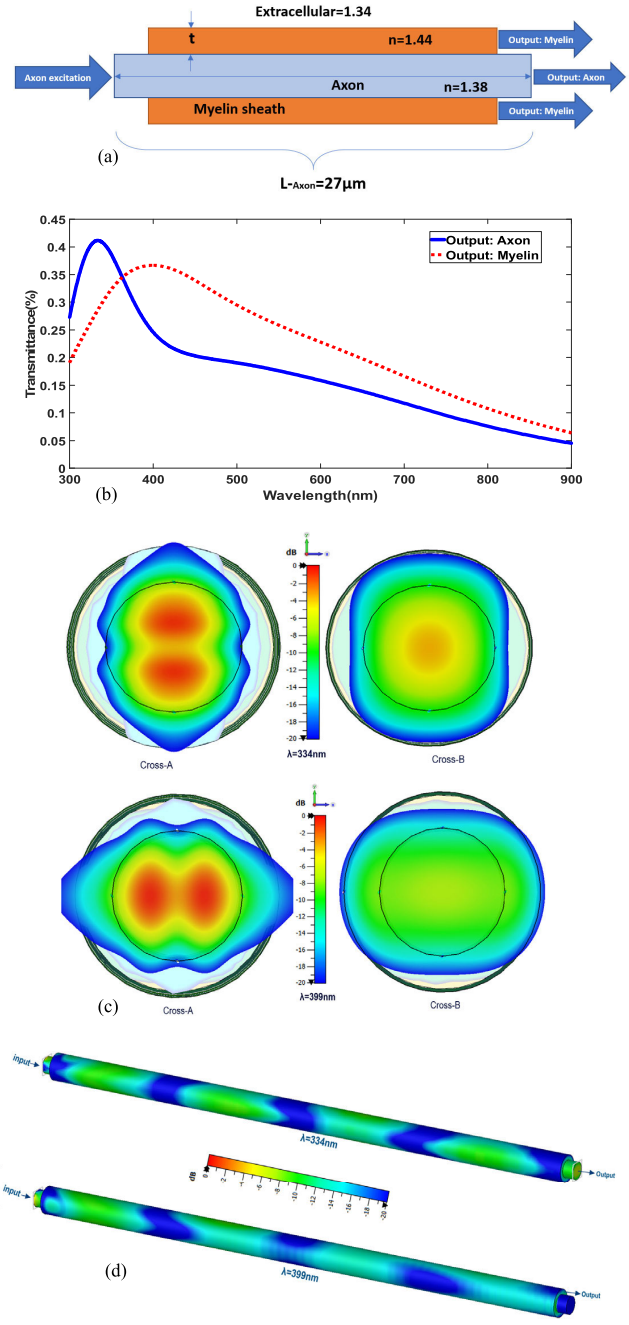

FIGURE 3. (a) Engineering model of nerve fiber, (b) Transmittance coefficient of the single nerve fiber with the different excitation ports, (c) Electric field distribution of cross-sections (A), (B) at $\lambda = 334$nm and $\lambda = 399$nm, (d)3D distribution of Electric field in the nerve fiber with axon output at $\lambda = 334$nm and myelin output at $\lambda = 399$nm.

presented structure, as illustrated in Fig. 4(a). The structure looks like the previous configuration, except that a paranode is inserted at the end of the architecture with a refractive index equal to the myelin (n = 1.44). In this step, the single segment of the nerve fiber is considered a lossless structure. Owing to the high absorbance of nerve cells in practice, we also evaluate nerve fibers in terms of lossy properties. In the available literature [31], there is no experimental data

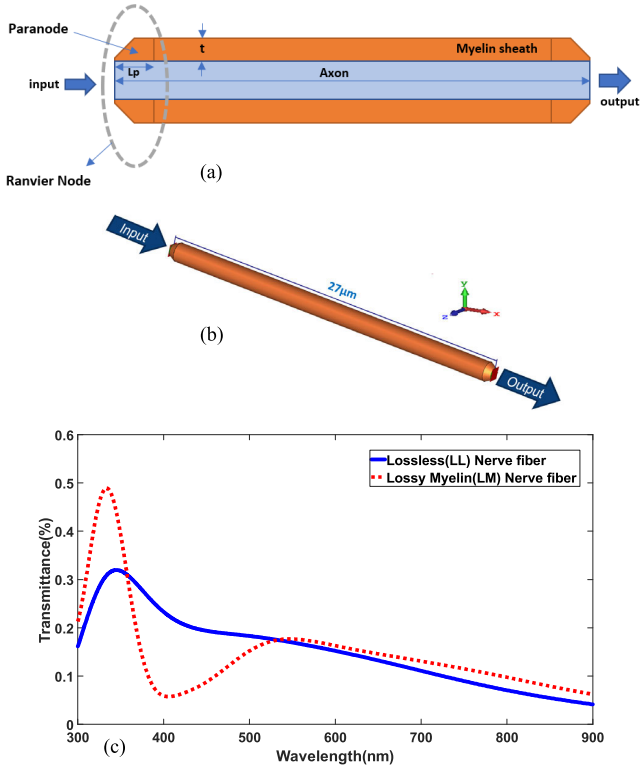

FIGURE 4. (a) Schematic of the Nerve fiber with Paranode, (b) the myelinated axon implemented in CST studio software (c)the calculated transmittance coefficient of myelinated axon in both the LL and LM tissues.

on the myelinated axon that perfectly present the lossy status of neurons. As such, it could be a valid assumption to estimate the myelin sheath as a fatty tissue [47], [48] because the myelin sheath is mostly composed of fatty substances. Thus, we approximate the optical behavior of the myelin sheath with a fatty tissue, which means the refractive index of myelin is considered as fat [49], [50]. The transmittance coefficient is then computed in both lossless (LL) and lossy myelin (LM) structures. The structure, implemented in CST Studio, is demonstrated in Fig. 4(b). The simulated results in Fig. 4(c) indicate that adding the paranode section leads to a remarkable drop in the transmittance coefficient, about 10 percent in the transmission peak. High diffraction due to the difference of refractive indices between the paranode and axon could be the reason for this drop when the photonic signal arrives in the axon. In the case of an LM structure, there is a sharp increase in the transmittance curve that may stem from constructive interactions of electromagnetic fields based on the modal index of the configuration. The peak distribution of the electromagnetic field in LL and LM structures is highlighted in Fig. 5(a),(b).

For more details concerning the influence of nerve fiber dimensions on light transmission, factors like myelin thickness and fiber length are considered. Correspondingly, their transmittance coefficients are calculated in LL and LM configurations. To study the myelin thickness, the g-ratio parameter is varied between 0.6, 0.7, and 0.78, while the radius

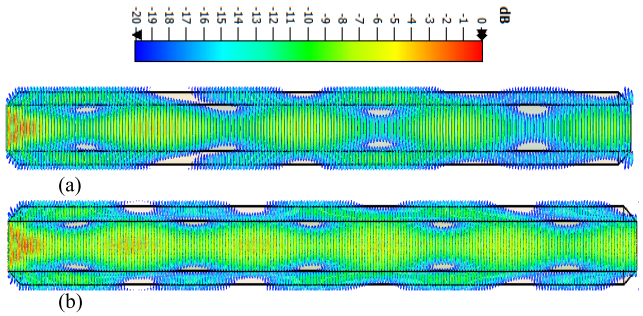

FIGURE 5. (a)The distribution of maximum Electric field in LL nerve fiber, $\lambda = 345$nm (b) The distribution of maximum Electric field in LM nerve fiber, $\lambda = 332$nm.

of the axon is consistently assumed to be 0.4μm. Under these changes, the myelin thickness changes to 0.533μm, 0.343μm, and 0.2256μm. Nerve fibers can operate as a multi-mode channel from an optoelectronic standpoint [51]. Hence, when photons are coupled to nerve fibers, they are decomposed to the modal components of tissue and propagated with specific velocities for each mode and corresponding cut-off frequencies. Changing the g-ratio setting causes a shift in the cut-off frequency of fiber channels affected by the diameter of the myelinated axon channel; therefore, spectral displacement on the transmission band of the nerve segment is tangible. Thicker myelin has the potential to confine more photons inside of the axon in lower wavelengths. Some fluctuations occur at the beginning of the nerve channel's transmission band, which stems from the profile variation of the nerve channel's electromagnetic field. The simulated results regarding the influence of g-ratio changes are illustrated in Fig.6(a),(b) in both LL and LM states.

Next, the effect of the segment length on the transmission of the photonic signal is described. In this case, the 27-μm length (the smallest measure) of the rat's nerve fiber is changed to 82μm (the average length) and 154μm (the most significant length) to evaluate photon transport in both LL and LM structures. In order to satisfy the assumption regarding the ratio of internodal length(L) and myelin sheath diameter(D) that is almost equal to 100 [36], we also consider the length of the nerve segment based on this ratio(L/D = 100) in simulations. By this hypothesis, the internodal length of configuration changes to 125.2μm, too. In the LL architecture, the transfer of the photonic signal along the nerve fiber is remarkably reduced by an increase in the length of the nerve channel, as shown in Fig. 7(a). The profile of the electro-optic fields accounts for some wrinkles in lower wavelengths when the length of the fiber channel is enlarged. An increase in fiber length leads to employing a modal dispersion to fibers. As such, wavelength components of each mode propagate on the different velocities, and signals on the output port are constructed by the time delay of the guided modes. Thus, signal distortions, like wrinkles, appear in the transmission band of the nerve fiber. In the LM structure, there is material dispersion as well as modal dispersion, as seen in Fig. 7(b). The influence of path loss on photonic signal transmission

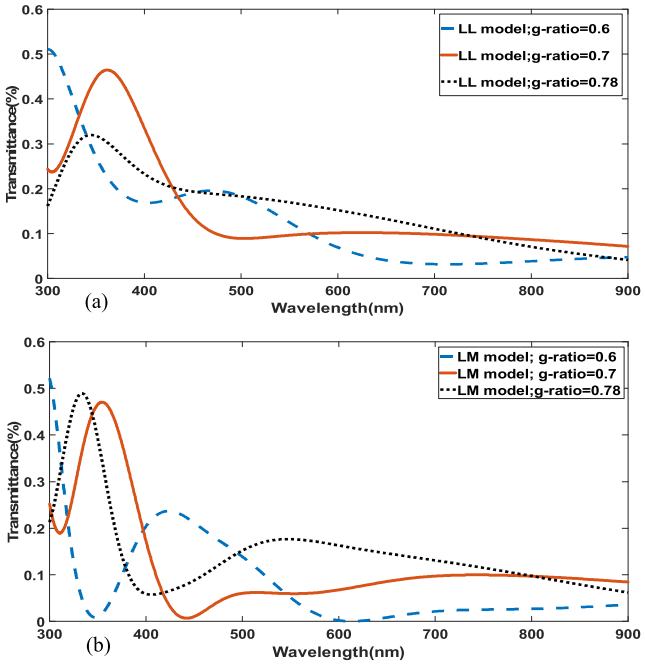

FIGURE 6. (a) the dependence of g-ratio changing on transmittance coefficient for LL nerve fiber, (b) the dependence of g-ratio changing on transmittance coefficient for LM nerve fiber.

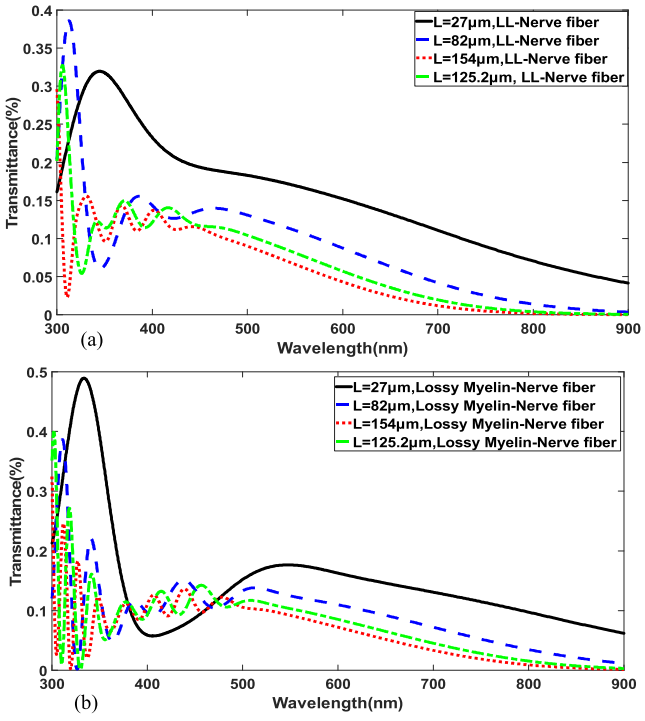

FIGURE 7. (a) the effect of nerve fiber length on transmittance coefficient for LL nerve fiber, (b) the impact of nerve fiber length on transmittance coefficient for LM nerve fiber.

is well specified. Interestingly, as shown in Fig.7, the optical behavior of the modeled nerve fiber shows that fiber channels in wavelengths under 500nm function like a multi-mode fiber, and modal dispersion plays a key role in creating distortion along with this range. In wavelengths higher than 500nm, the

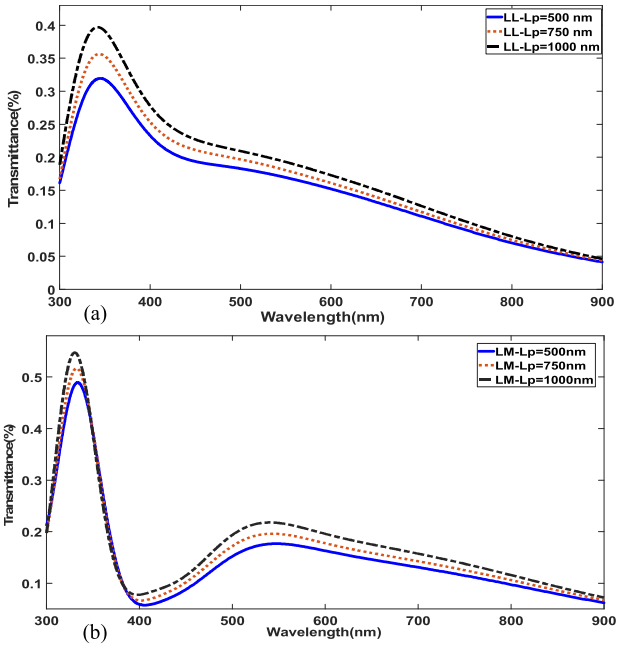

FIGURE 8. (a)The effect of paranode length on transmittance for (a) LL nerve fiber,(b) LM nerve fiber.

fiber channel operates like a single-mode fiber. The path loss of nerve fibers is well observed in wavelengths greater than 500nm.

Afterward, we focus on the paranodal zone of the nerve segment placed in the first and end of the nerve segment. To find the impact of the paranode length on transmittance, variation of paranode's physical size is simulated. For this, the paranode length on both sides of the nerve segment is changed to750nm and 1000nm. The simulated results in Fig.8(a),(b) show an increase in paranode length causes more energy transmits inside the axonal route of the nerve segment for both LL and LM structures. In fact, increase in the paranode size, new modes are generated that have a constructive potential and enhance the photonic signaling in the axon. Forward reflectance due to new modes generated leads more photons are transmitted when the photonic signal arrives at a longer length of the paranodal zone. As an interesting point, it seems the paranode area can adjust the signal level at the arrivals of axonal routes and might function as an adaptor. A paranode with proper length can have a constructive effect on photon transition inside the axonal zone based on our simulations. For further details, an in-depth analysis of the paranodal zone's impact on the photonic signal transmission in a cross-section of the nerve fibers can be found in [35].

The effect of the Ranvier node is simulated to understand its influence on the optical spectrum in the transmission band. At the start, the length of the structure is 27μm for simulation, as shown in Fig.9(a). We aim to assess the size effect of the Ranvier gap on photon transitions. The biological features of the Ranvier node are ignored in this section, and the refractive index of the Ranvier area is equal to 1.38 [35]. The size of the Ranvier gap for the rat is given as 0.7μm, 1.08μm, and 1.4μm [8]. The simulated results for LL and

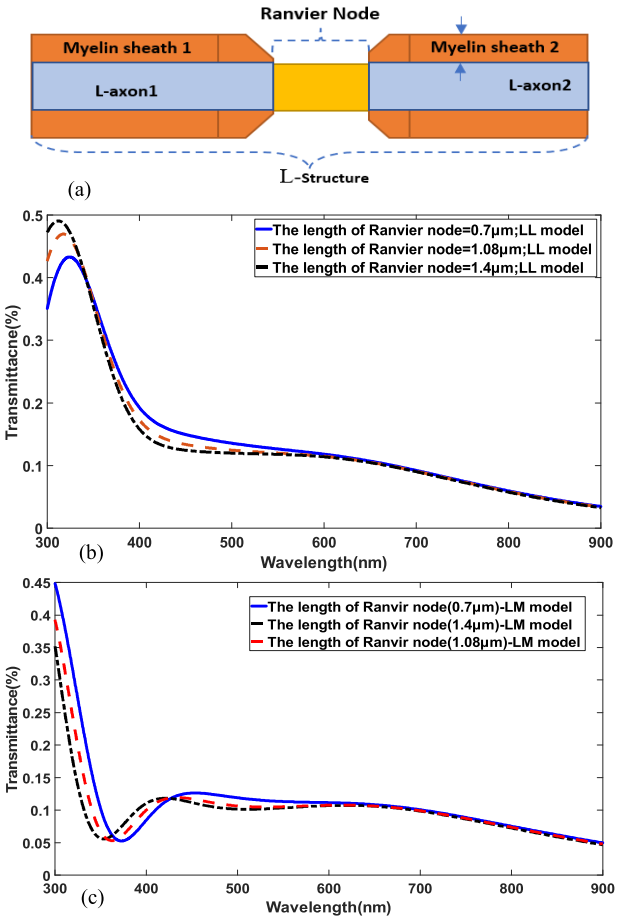

FIGURE 9. (a) the schematic of Ranvier node between the 2-nerve segment of nerve fiber, (b) the effect of Ranvier node length on transmittance coefficient for LL nerve fiber(c) the effect of Ranvier node length on transmittance coefficient for LM nerve fiber.

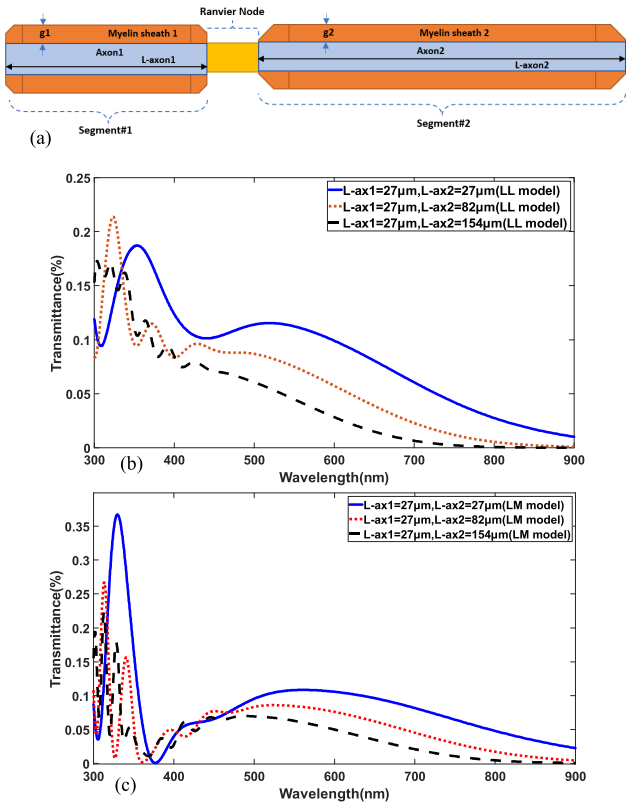

FIGURE 10. (a)A schematic of two myelinated axon segments of nerve fiber which are placed (b) The influence of adding myelinated axon segment on transmittance coefficient in lossless nerve fiber, (c)The influence of adding myelinated axon segment on transmittance coefficient in lossy nerve fiber continuously.

LM structures indicate that there is a downward trend in all results, as demonstrated in Fig.9(b),(c), which are derived from becoming close to the cut-off wavelength. A blueshift happens with an increase in the dimension of the Ranvier node, which is a well-known indicator in spectroscopy measurements. This blue shift is due to the variation of the structure's optical properties derived from manipulating the mode index of the bounded medium[52]. In detail, adding the Ranvier node between segments and changing size in the architecture of Fig.9(a) causes new modes to be imposed on the electromagnetic radiation profile of construction. On this basis, simulation modes of the proposed configuration in lower frequency enhance the guided signal inside fibers with more than 40 percent of transmission and have a constructive effect on the photonic signal in the output port.

In attempting to investigate light attenuation in terms of two-segment connections and path loss evaluation, the second segment is connected to the configuration, as shown in Fig. 10(a). Our aim is to perceive how photons are attenuated on segments of a nerve fiber. From an architectural aspect, two segments of the myelinated axon as parts of the nerve fiber are chosen. One of the sections is sized as large as 27μm, and another one is sized at 27μm, 82μm, and 154μm for both LL and LM structures. All physical parameters regarding the presented two-segment structure for both states look like the previous arrangements. The transmittance factor is decreased when the number of sectors and the length of the nerve fiber are extended, as indicated in Fig.10(b),(c). In practice, the attenuated signals are enhanced in the Ranvier node through active ionic amplifications [53]–[56], which is not considered here. Structural manipulation causes modal dispersion on the structure; therefore, the interconnection of two nerve segments across the fiber creates a remarkable distortion on the spectral response due to new generated modes and path loss. In the LM architecture, as seen in Fig.9(c), myelin dispersion, in addition to modal dispersion, is also motivated, and severe fluctuations appear in the transmission band.

B. DEMYELINATION EFFECT ON PHOTONIC TRANSITION IN MYELINATED AXON

As established, the myelin sheath is the most important part of the nerve fiber in terms of transmitting signals and serving as an insulator. The insulation in the myelin sheath of neurons enhances signal continuity and maintains living nerve cells. Defection of the myelin sheath leads to lost nerve pulses inside the neural network of the brain. Subsequently, intracellular communication is damaged, and the nerve cell is dead.

In many cases, the demyelination of a nerve fiber causes a wide range of disorders in the central nervous system, such as stroke, spinal cord injury, and MS. For instance, in MS, the myelin sheath is destroyed through the attack of the body's immune system [57], [58]. Furthermore, myelin is introduced as a place for signal transmission in the intracellular communication network; hence demyelination causes a signaling discontinuity between neurons. In this regard, scientists acquire some knowledge using gold nanorods and silicon nanoparticles to improve nerve activity, and repair signaling discontinuity stemmed from demyelination inside of nerve fibers [59], [60]. For a biophysical survey, we concentrate on the effect of the defected myelin of LL nerve fiber and investigate its transmittance coefficient in this section. First, a defection as demyelination is built onto the layer of the myelin sheath of an ordinary nerve segment as great as 1.8μm in length (L_D) and 0.113μm in-depth(t/2), as demonstrated in Fig.10(a). This demyelination is positioned in the first part of the nerve fiber segment, and other dimensions remain unchanged. Then, in order to investigate the length effect of demyelination, it is changed to 3.7μm and 5.4μm. The simulated results in Fig.11(b) imply that photon transmission is affected by demyelination, and the transmittance coefficient is reduced in this situation. This effect is rooted in the light diffraction in the demyelinated region, leading to fewer photon passes along the axon. In addition, demyelination leads to generate new propagation modes that influence signal transmission. In fact, when the demyelination length changes to 3.7μm, transmittance face with more drop between 320 nm to 550 nm, while the length varies to 5.4μm, new modes produced under this change cause a constructive effect at the same band in terms of signal transmission relative to length 3.7μm, so transmittance goes up, as illustrated in Fig.11.(b). In the following, demyelination length is fixed to 5.4μm, then the depth of defection is changed from 113 nm to 75.2 nm and 45.13 nm. The simulated results in Fig.11(c) shows that more photon transmits through axon once demyelination depth becomes smaller. At wavelength under 320 nm, we can see an improvement in transmittance due to newly guided modes' constructive performance and forward reflectance enhancement.

Afterward, the location of demyelination is shifted to the middle of the nerve segment, as demonstrated in Fig.12(a). Again, the effect of length and depth of demyelination is studied in the situation. First, the length of demyelination is considered 1.8μm, 3.7μm, and 5.4μm, while the depth of demyelination is continuously 113nm. In this context, the simulated results in Fig.12(b) indicate that transmittance increases about 10-15 percent even more than the normal nerve fiber under 400nm when the length of demyelination is 1.8μm and 3.7μm rooted in the constructive effect of guided modes produced. In other words, forward reflectance due to demyelination enhances the passing photonic signal inside the axon in wavelengths under 400nm. In contrast, at the same wavelength for a demyelination length of 5.4μm, there is a 10-percent drop in transmittance. This means the intensity of

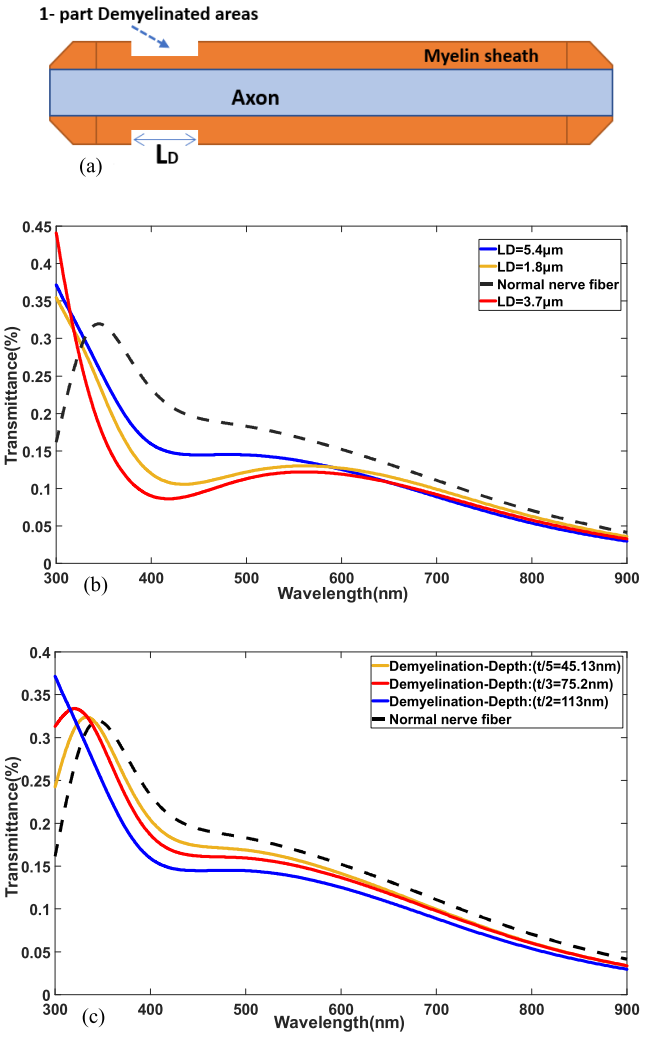

FIGURE 11. (a)A schematic model of the demyelinated axon (demyelination creates in the first of nerve fiber), (b) the impact of demyelinated length on transmittance (Depth = 113nm), (c) the impact of demyelinated depth on transmittance ($L_D = 5.4\mu$m).

backward reflectance due to demyelination plays a predominant role, and a less photonic signal is confined inside the axonal route. Next, the demyelination length is considered 5.4μm, and the depth of demyelination is changed from 113nm to 75.2nm and 45.13nm. As shown in Fig.12(c), transmittance in more depth of demyelination follows a downward trend, and reflectance negatively impacts photons passing inside the axon.

For further study, the number of demyelination is increased to 3 positions with $L_D = 5.4\mu$m and depth of 113nm, as illustrated in Fig.13(a). We aim to find the optical behavior of the demyelinated nerve segment when the number of demyelinations is increased. As resulted in Fig13(b), an increase in the number of demyelination areas on nerve fiber reduces the level of photonic signal transition considerably in a wide wavelength range. However, a constructive effect due to multi-mode reflection at wavelengths under 320 nm creates a tangible amplification of about 10 percent. As a result, the destructive or constructive effect of nerve fiber's multi-mode

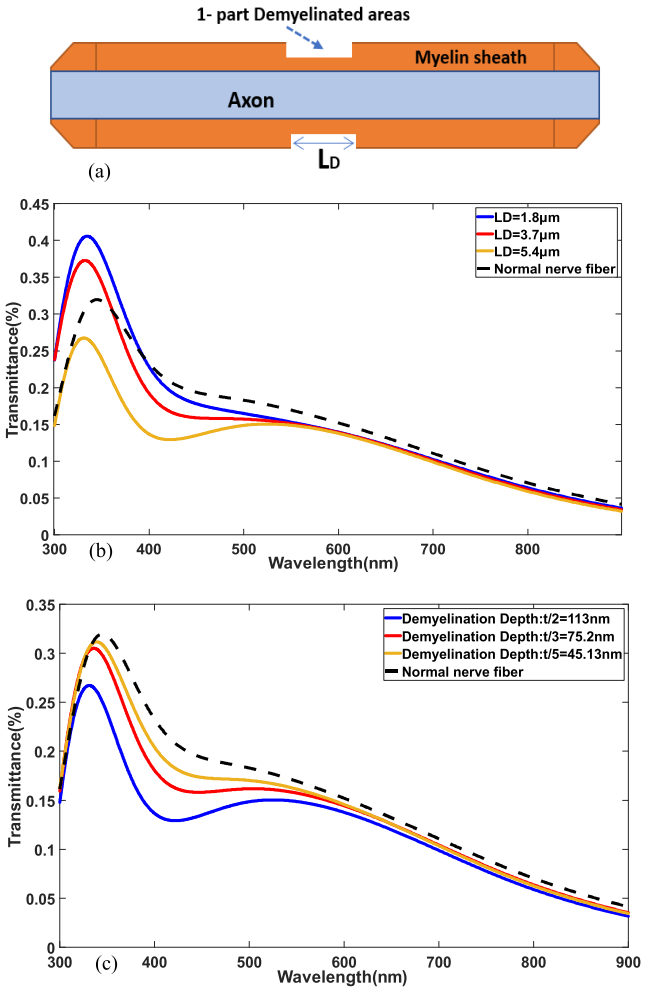

FIGURE 12. (a)A schematic model of the demyelinated axon(demyelination creates in the middle of nerve fiber), (b) the impact of demyelinated length on transmittance(Depth = 113nm), (c) the impact of demyelinated depth on transmittance($L_D = 5.4\mu$m).

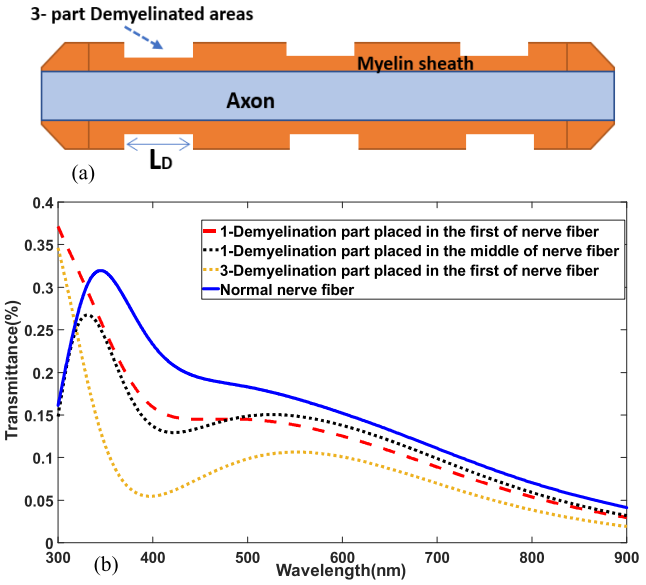

FIGURE 13. (a) A schematic model of the demyelinated axon (three demyelinations create on nerve fiber), (b) the impact of the increase in the number of demyelinated areas on nerve fiber's transmittance.

reflection plays a key role in weakening and amplifying transmittance inside the nerve fiber's axonal routes. Most attenuation appears in a spectral range between 320 nm and 550nm.

C. ENHANCEMENT OF PHOTONIC TRANSMISSION IN NERVE FIBERS BY NANOPARTICLES AND NANORODS

As shown in the prior section, nerve fiber's demyelination affects the photonic signal transmission while crossing the axon. This effect might be constructive or destructive, depending on the axon channel's reflectance, whether it is made forward or backward. Destructive impact of reflectance causes a photonic signal attenuation in the transmission band. As a remedy to this signal drop, it is necessary to manipulate the optical characteristics of nerve configuration to modify photonic transition. Using nanoparticles to apply for nerve fiber repairment is overgrowing, and scientists are focusing on this area by injecting nanoparticles into the body [61], [62]. Our idea behind this approach is to employ nanoparticles in the extracellular medium around the demyelinated area that can change the effective refractive index of configuration. Consequently, more photons remain inside the axon. In order to prove this method based on an exact simulation, a demyelinated axon with a size of 5.4μm in length and 113nm in depth is chosen. The spherical nanoparticle is put in the demyelination position, as illustrated in Fig.14(a). The nanoparticle's radius is considered 50 nm. Since a single segment of nerve fiber looks like the compound optical waveguide in terms of configuration, it is important to use nanoparticles with a high refractive index to enhance guided mode inside the axonal route. The first choice is silicon nanoparticle, which possesses a high refractive index in the considered range. Since silicon has a very high combinability with the available oxygen in the extracellular medium, so silica is selected as the next nanoparticle for simulation. Silica counts as a biocompatible element as an implant inside the body, as well. A core-shell nanoparticle composed of Au(core)/Silica(shell) is selected because this kind of nanoparticle has great controllability compared to other options. In order to describe the refractive index of nanoparticles, the updated data in CST's library has been used in the simulations, which are also available in [63], [64]. The simulated results in fig.14(b) related to these nanoparticles show the transmittance curve of the demyelinated axon goes up after the injection of nanoparticles. The highest shift belongs to the perturbation of silicon nanoparticles that transmittance is increased by almost 10 percent. Silica quantum dot(QD) perturbation and Au/silica core sell nanoparticle also improve the photonic signal transmission by means of manipulating the refractive index of extracellular medium that means the effective refractive index (modal index) changes and the guided mode of the demyelinated axon enhances. The amount of this amplification is also different between 5-10 percent from 320nm to 650nm, as seen in Fig.14(b). Following, in order to evaluate the size effect of silicon

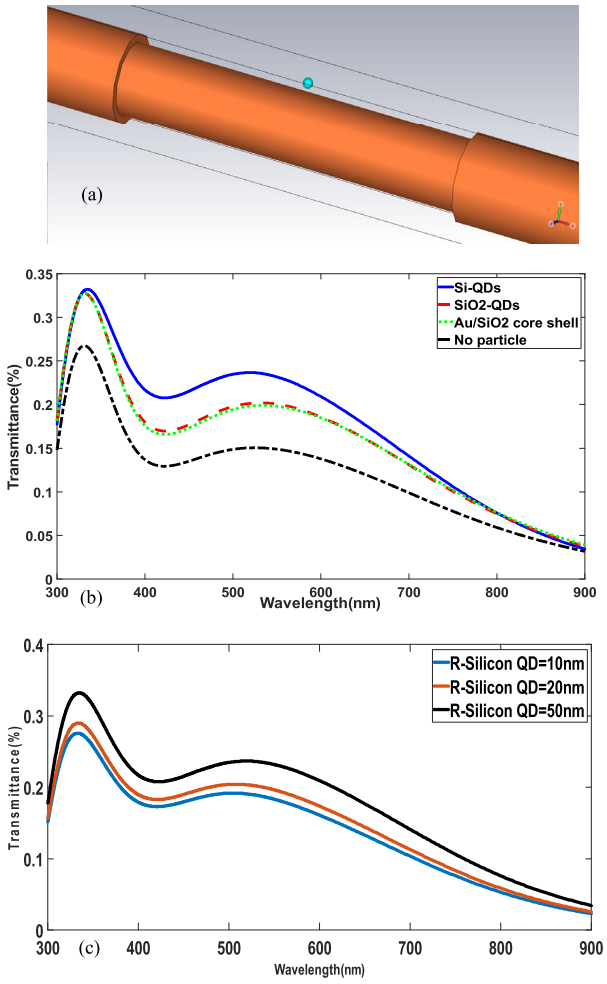

FIGURE 14. **(a)Schematic of demyelinated axon associated with single silicon QD injected in demyelinated area, (b) Comparison of demyelinated axon's transmittance via employing different nanoparticles with the radius of 50nm, (c) The size impact of single silicon QD injected inside the demyelinated area on transmittance.**

quantum dot(QD) on the transmittance, the size of silicon QDs varies in scales: 10nm, 20nm, and 50nm. As seen in Fig.14(c), the increase in the size of silicon QD enhances the photon transition, which is rooted in the positive performance of the effective refractive index in confining electromagnetic fields across axonal route when the perturbation of QDs is extended.

Then, since it is not possible to inject silicon QDs singly, a configuration of 12 silicon QDs with radii of 50nm is placed in a ring surrounding the demyelinated space of the nerve fiber, as illustrated in Fig. 15(a). The spectra in Fig.15(b) indicate that the transmittance is significantly improved over the transmission band, especially for wavelengths less than 400 nm. For more precise analysis, a combination of silicon QDs with various dimensions of 10nm and 50nm are located close to each other surrounding the demyelination to evaluate the effect of the size distribution of silicon QDs on the transmission band, as shown in Fig. 15(c). Fig. 15(d) illustrates that photonic signaling is enhanced impressively in wavelengths lower than 380nm, and a dramatic improvement in the photon transition is observed on the transmission band.

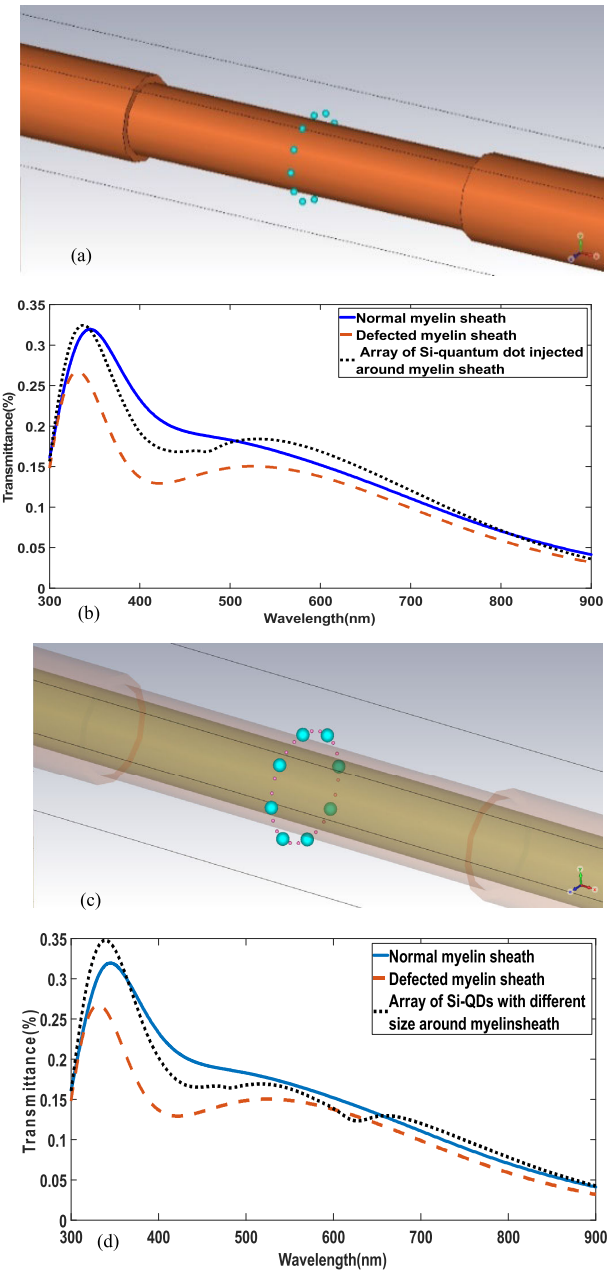

FIGURE 15. **(a)Schematic of demyelinated axon associated with silicon QD array injected in the demyelinated area, (b) the effect of silicon QD array with the radius of 50nm on demyelinated axon's transmittance, (c) Schematic of the demyelinated axon with silicon QD array with the size of 50nm,10nm,(d) the effect of silicon QD array with the different radiuses of 50nm and 10nm on demyelinated axon's transmittance.**

Afterward, a nanorod structure is also examined as another similar suggestion, as seen in Fig.16(a). Silicon, silica, and gold are the ingredients of the nanorod. The size of the proposed nanorod is 100nm in diameter and 540nm in height. Like before, the goal is to calculate the transmittance of the demyelinated nerve segment. The simulated results in fig.16(b) demonstrate that the insertion of nanorod can improve transmittance by more than 10 percent at

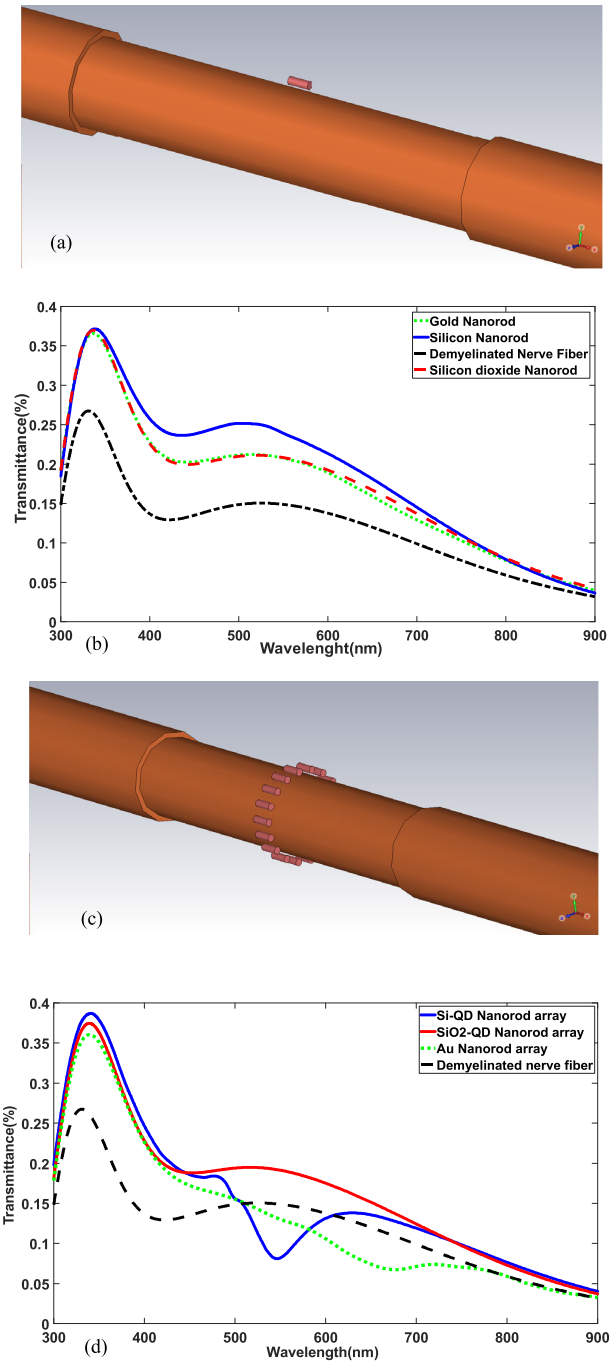

FIGURE 16. **(a)Schematic of single nanorod injected in the demyelinated area, (b) the calculated transmittance for different single nanorod injected in the demyelinated area, (c)Schematic of nanorod array placed around demyelinated nerve fiber(d) the calculated transmittance of demyelinated nerve fiber using Nanorod array composed of different materials.**

wavelengths under 550nm, and among those, silicon possesses the highest value. In other words, adding nanorod and changing the effective refractive index of nerve fiber structure generate the guided modes inside the axon, and more photons are confined inside the axon. Next, the number of nanorods is increased to 18 elements surrounding the demyelinated area, as shown in Fig.16(c). Nanorod array levels up transmittance curves significantly at lower wavelengths in which this extra value is about 15 percent, as seen in Fig.16(d). In addition, a dramatic drop happens in the transmittance curve of silicon nanorod array at wavelengths between 500nm to 600nm, which gets back to the destructive impact of the structure's effective refractive index and then guided mode of axon decreases. This optical behavior occurs for a gold nanorod array between 500nm to 780 nm, as well. As a result, it is evident that by placing nanoparticles and nanorods, it is possible to improve the transmittance level of a demyelinated axon that is very tangible at wavelengths lower than 500nm.

IV. CONCLUSION

In our work, photonic transmission through the nerve fiber is studied using biophysical established concepts. Although we faced some limitations as the absence of lossy experimental data concerning refractive indexes of nerve fiber's ingredients and ultra-weak biophotonic signal that detecting it is a challenge; however, our findings provide a model of photonic transition along axonal routes between neurons, which is able to promote signaling in the neuronal networks of the brain. We demonstrated that nerve fibers could pass photonic signals through myelinated axons and analyze it via full-wave numerical computations. Based on the extracted results, the nerve fiber's propagating mode is predominant relative to the nerve fiber segment's guided mode due to the lesser value of the modal index of nerve segments compared to the refractive index of the myelin sheath layer, which means the guided wave decays. By attention to the size and length of the nerve fiber, we found that the percentage of transmitted photons can be affected by the dimensional change, causing mode dispersion. Besides, we engineered the demyelination impact of nerve fibers considered as a defect that could generate new modes in the electromagnetic field profile, causing a destructive or constructive effect on transmittance. In most of the spectral ranges, demyelination's destructive effect plays a dominant role in the transmission band, and transmittance is attenuated.

As a technical solution for this challenge, we analyzed a nano-approach based on the perturbation of QDs and nanorods to manipulate the nerve configuration's modal index. This proved nanoparticles or nanorods inserted around the demyelinated region change the effective refractive index of nerve configuration in alignment with the enhancement of the photonic signal's guided mode, thus increasing in transmittance appears. As a result, the nanoparticles can enhance photon transmission in a wide range of visible-infrared bands between 300nm and 900nm in the nerve fibers. This approach establishes a preliminary approximate nerve model that can promote new studies in cell-level signaling, computational neuroscience, and deep brain stimulation based on nanophotonic communications concepts.

REFERENCES

[1] S. Wirdatmadja, P. Johari, S. Balasubramaniam, Y. Bae, M. Stachowiak, and J. Jornet, "Light propagation analysis in nervous tissue for wireless optogenetic nanonetworks," *Proc. SPIE*, vol. 1048, Feb. 2018, Art. no. 104820R.

[2] R. Habibey, K. Sharma, A. Swiersy, and V. Busskamp, "Optogenetics for neural transplant manipulation and functional analysis," *Biochem. Biophys. Res. Commun.*, vol. 527, no. 2, pp. 343–349, Jun. 2020, doi: 10.1016/j.bbrc.2020.01.141.

[3] M. G. Christiansen, A. W. Senko, and P. Anikeeva, "Magnetic strategies for nervous system control," (in eng), *Annu. Rev. Neurosci.*, vol. 42, no. 1, pp. 271–293, Jul. 2019, doi: 10.1146/annurev-neuro-070918-050241.

[4] J. Proft and N. Weiss, "From opto-to radio-genetics: A switch in the wavelength," (in eng), *Communicative Integrative Biol.*, vol. 5, no. 3, pp. 227–229, May 2012, doi: 10.4161/cib.21148.

[5] P. P. Sordillo and L. A. Sordillo, "The mystery of chemotherapy brain: Kynurenines, tubulin and biophoton release," (in eng), *Anticancer Res.*, vol. 40, no. 3, pp. 1189–1200, Mar. 2020, doi: 10.21873/anticanres.14061.

[6] M. Cifra, J. Z. Fields, and A. Farhadi, "Electromagnetic cellular interactions," *Prog. Biophys. Mol. Biol.*, vol. 105, no. 3, pp. 223–246, May 2011, doi: 10.1016/j.pbiomolbio.2010.07.003.

[7] V. Salari, F. Scholkmann, R. L. P. Vimal, N. Császár, M. Aslani, and I. Bókkon, "Phosphenes, retinal discrete dark noise, negative afterimages and retinogeniculate projections: A new explanatory framework based on endogenous ocular luminescence," *Prog. Retinal Eye Res.*, vol. 60, pp. 101–119, Sep. 2017, doi: 10.1016/j.preteyeres.2017.07.001.

[8] I. L. Arancibia-Cárcamo, M. C. Ford, L. Cossell, K. Ishida, K. Tohyama, and D. Attwell, "Node of ranvier length as a potential regulator of myelinated axon conduction speed," (in eng), *eLife*, vol. 6, Jan. 2017, Art. no. e23329, doi: 10.7554/eLife.23329.

[9] R. Tang and J. Dai, "Biophoton signal transmission and processing in the brain," *J. Photochem. Photobiol. B, Biol.*, vol. 139, pp. 71–75, Oct. 2014, doi: 10.1016/j.jphotobiol.2013.12.008.

[10] Z. Wang, N. Wang, Z. Li, F. Xiao, and J. Dai, "Human high intelligence is involved in spectral redshift of biophotonic activities in the brain," (in eng), *Proc. Nat. Acad. Sci. USA*, vol. 113, no. 31, pp. 8753–8758, Aug. 2016, doi: 10.1073/pnas.1604855113.

[11] D. Chaudhury *et al.*, "Rapid regulation of depression-related behaviours by control of midbrain dopamine neurons," *Nature*, vol. 493, no. 7433, pp. 532–536, Jan. 2013, doi: 10.1038/nature11713.

[12] H. Wang, C. Magnain, S. Sakadžić, B. Fischl, and D. A. Boas, "Characterizing the optical properties of human brain tissue with high numerical aperture optical coherence tomography," (in eng), *Biomed. Opt. Exp.*, vol. 8, no. 12, pp. 5617–5636, 2017, doi: 10.1364/BOE.8.005617.

[13] K. Park and S. Weiss, "Design rules for membrane-embedded voltage-sensing nanoparticles," *Biophys. J.*, vol. 112, no. 4, pp. 703–713, Feb. 2017, doi: 10.1016/j.bpj.2016.12.047.

[14] F. Grass, H. Klima, and S. Kasper, "Biophotons, microtubules and CNS, is our brain a 'holographic computer?'" *Med. Hypotheses*, vol. 62, no. 2, pp. 169–172, 2004, doi: 10.1016/S0306-9877(03)00308-6.

[15] Y. Isojima, T. Isoshima, K. Nagai, K. Kikuchi, and H. Nakagawa, "Ultraweak biochemiluminescence detected from rat hippocampal slices," *NeuroReport*, vol. 6, no. 4, pp. 658–660, Mar. 1995.

[16] M. Kobayashi, M. Takeda, T. Sato, Y. Yamazaki, K. Kaneko, K.-I. Ito, H. Kato, and H. Inaba, "*In vivo* imaging of spontaneous ultraweak photon emission from a rat's brain correlated with cerebral energy metabolism and oxidative stress," *Neurosci. Res.*, vol. 34, no. 2, pp. 103–113, 1999, doi: 10.1016/S0168-0102(99)00040-1.

[17] Y. Sun, C. Wang, and J. Dai, "Biophotons as neural communication signals demonstrated by *in situ* biophoton autography," *Photochem. Photobiolog. Sci.*, vol. 9, no. 3, pp. 315–322, 2010, doi: 10.1039/B9PP00125E.

[18] Y. Kataoka, Y. Cui, A. Yamagata, M. Niigaki, T. Hirohata, N. Oishi, and Y. Watanabe, "Activity-dependent neural tissue oxidation emits intrinsic ultraweak photons," (in eng), *Biochem. Biophys. Res. Commun.*, vol. 285, no. 4, pp. 1007–1011, Jul. 2001, doi: 10.1006/bbrc.2001.5285.

[19] V. Salari, H. Valian, H. Bassereh, I. Bókkon, and A. Barkhordari, "Ultraweak photon emission in the brain," *J. Integrative Neurosci.*, vol. 14, no. 3, pp. 419–429, Sep. 2015, doi: 10.1142/s0219635215300012.

[20] B. P. Watts, M. Barnard, and J. F. Turrens, "Peroxynitrite-dependent chemiluminescence of amino acids, proteins, and intact cells," *Arch. Biochem. Biophys.*, vol. 317, no. 2, pp. 324–330, Mar. 1995, doi: 10.1006/abbi.1995.1170.

[21] B. Bordoni, F. Marelli, B. Morabito, and B. Sacconi, "Emission of biophotons and adjustable sounds by the fascial system: Review and reflections for manual therapy," *J. Evidence-Based Integrative Med.*, vol. 23, 2018, Art. no. 2515690X17750750.

[22] M. Rahnama, J. A. Tuszynski, I. Bókkon, M. Cifra, P. Sardar, and V. Salari, "Emission of mitochondrial biophotons and their effect on electrical activity of membrane via microtubules," *J. Integrative Neurosci.*, vol. 10, no. 1, pp. 65–88, Mar. 2011, doi: 10.1142/s0219635211002622.

[23] F. Scholkmann, "Long range physical cell-to-cell signalling via mitochondria inside membrane nanotubes: A hypothesis," (in eng), *Theor. Biol. Med. Model.*, vol. 13, no. 1, p. 16, Dec. 2016, doi: 10.1186/s12976-016-0042-5.

[24] M. Valko, D. Leibfritz, J. Moncol, M. T. D. Cronin, M. Mazur, and J. Telser, "Free radicals and antioxidants in normal physiological functions and human disease," *Int. J. Biochem. Cell Biol.*, vol. 39, no. 1, pp. 44–84, Jan. 2007, doi: 10.1016/j.biocel.2006.07.001.

[25] A. Zangari, D. Micheli, R. Galeazzi, A. Tozzi, V. Balzano, G. Bellavia, and M. E. Caristo, "Photons detected in the active nerve by photographic technique," *Sci. Rep.*, vol. 11, no. 1, p. 3022, Dec. 2021, doi: 10.1038/s41598-021-82622-5.

[26] Y. Liu, K. Wu, C. Liu, G. Cui, C. Chang, and G. Liu, "Amplification of terahertz/infrared field at the nodes of ranvier for myelinated nerve," *Sci. China Phys., Mech. Astron.*, vol. 63, no. 7, Jul. 2020, Art. no. 274211, doi: 10.1007/s11433-019-1530-2.

[27] S. Wirdatmadja, P. Johari, A. Desai, Y. Bae, E. K. Stachowiak, M. K. Stachowiak, J. M. Jornet, and S. Balasubramaniam, "Analysis of light propagation on physiological properties of neurons for nanoscale optogenetics," *IEEE Trans. Neural Syst. Rehabil. Eng.*, vol. 27, no. 2, pp. 108–117, Feb. 2019, doi: 10.1109/TNSRE.2019.2891271.

[28] G. Liu, C. Chang, Z. Qiao, K. Wu, Z. Zhu, G. Cui, W. Peng, Y. Tang, J. Li, and C. Fan, "Myelin sheath as a dielectric waveguide for signal propagation in the mid-infrared to terahertz spectral range," *Adv. Funct. Mater.*, vol. 29, no. 7, Feb. 2019, Art. no. 1807862, doi: 10.1002/adfm.201807862.

[29] R. Tang and J. Dai, "Spatiotemporal imaging of glutamate-induced biophotonic activities and transmission in neural circuits," (in eng), *PLoS ONE*, vol. 9, no. 1, Jan. 2014, Art. no. e85643, doi: 10.1371/journal.pone.0085643.

[30] K. M. Hebeda, T. Menovsky, J. F. Beek, J. G. Wolbers, and M. J. C. van Gemert, "Light propagation in the brain depends on nerve fiber orientation," *Neurosurgery*, vol. 35, no. 4, pp. 720–724, Oct. 1994, doi: 10.1227/00006123-199410000-00019.

[31] S. Kumar, K. Boone, J. Tuszynski, P. Barclay, and C. Simon, "Possible existence of optical communication channels in the brain," *Sci. Rep.*, vol. 6, no. 1, p. 36508, Dec. 2016, doi: 10.1038/srep36508.

[32] V. Tuchin, "Tissue optics and photonics: Light-tissue interaction II," *J. Biomed. Photon. Eng.*, vol. 2, no. 3, 2016, Art. no. 030201, doi: 10.18287/jbpe16.02.030201.

[33] R. M. Stassart, W. Möbius, K.-A. Nave, and J. M. Edgar, "The axon-myelin unit in development and degenerative disease," (in English), *Frontiers Neurosci.*, vol. 12, p. 467, Jul. 2018, doi: 10.3389/fnins.2018.00467.

[34] K. Susuki, "Myelin: A specialized membrane for cell communication," *Nature Educ.*, vol. 3, no. 9, p. 59, 2010.

[35] A. Zangari, D. Micheli, R. Galeazzi, and A. Tozzi, "Node of ranvier as an array of bio-nanoantennas for infrared communication in nerve tissue," *Sci. Rep.*, vol. 8, no. 1, p. 539, Dec. 2018, doi: 10.1038/s41598-017-18866-x.

[36] M. C. Ford, O. Alexandrova, L. Cossell, A. Stange-Marten, J. Sinclair, C. Kopp-Scheinpflug, M. Pecka, D. Attwell, and B. Grothe, "Tuning of ranvier node and internode properties in myelinated axons to adjust action potential timing," *Nature Commun.*, vol. 6, no. 1, p. 8073, Nov. 2015, doi: 10.1038/ncomms9073.

[37] W. A. Jacak, "Propagation of collective surface plasmons in linear periodic ionic structures: Plasmon polariton mechanism of saltatory conduction in axons," *J. Phys. Chem. C*, vol. 119, no. 18, pp. 10015–10030, May 2015, doi: 10.1021/acs.jpcc.5b02418.

[38] J. Jacak and W. Jacak, "Plasmons and plasmon–polaritons in finite ionic systems: Toward soft-plasmonics of confined electrolyte structures," *Appl. Sci.*, vol. 9, no. 6, p. 1159, Mar. 2019, doi: 10.3390/app9061159.

[39] B. Song and Y. Shu, "Cell vibron polariton resonantly self-confined in the myelin sheath of nerve," *Nano Res.*, vol. 13, no. 1, pp. 38–44, Jan. 2020, doi: 10.1007/s12274-019-2568-4.

[40] X. Zhang and L. Jiang, "Quantum-confined ion superfluid in nerve signal transmission," *Nano Res.*, vol. 12, no. 6, pp. 1219–1221, Jun. 2019, doi: 10.1007/s12274-019-2281-3.

[41] I. P. Antonov, A. V. Goroshkov, V. N. Kalyunov, I. V. Markhvida, A. S. Rubanov, and L. V. Tanin, "Measurement of the radial distribution of the refractive index of the Schwann's sheath and the axon of a myelinated nerve fiber *in vivo*," *J. Appl. Spectrosc.*, vol. 39, no. 1, pp. 822–824, Jul. 1983.

[42] Z. Wang, M. Gillette, I. S. Chun, X. Li, Z. Y. Ong, E. Pop, and L. Millet, "Topography and refractometry of nanostructures using spatial light interference microscopy," *Opt. Lett.*, vol. 35, no. 2, pp. 208–210, 2010.
[43] V. V. Tuchin, I. L. Maksimova, D. A. Zimnyakov, I. L. Kon, A. H. Mavlyutov, and A. A. Mishin, "Light propagation in tissues with controlled optical properties," *J. Biomed. Opt.*, vol. 2, no. 4, pp. 401–417, 1997.
[44] G. P. Agrawal, *Fiber-Optic Communication Systems*. Hoboken, NJ, USA: Wiley, 2012.
[45] K. Okamoto, "Optical fibers," in *Fundamentals of Optical Waveguides*, K. Okamoto Ed., 2nd ed. Burlington, VT, USA: Academic, 2006, ch. 3, pp. 157–158.
[46] M. Jibu, S. Hagan, S. R. Hameroff, K. H. Pribram, and K. Yasue, "Quantum optical coherence in cytoskeletal microtubules: Implications for brain function," *Biosystems*, vol. 32, no. 3, pp. 195–209, 1994, doi: 10.1016/0303-2647(94)90043-4.
[47] R. J. Colello, "Myelin," in *Encyclopedia of Clinical Neuropsychology*, J. S. Kreutzer, J. DeLuca, and B. Caplan, Eds. New York, NY, USA: Springer, 2011, pp. 1690–1691.
[48] Y. Poitelon, A. M. Kopec, and S. Belin, "Myelin fat facts: An overview of lipids and fatty acid metabolism," (in eng), *Cells*, vol. 9, no. 4, p. 812, Mar. 2020, doi: 10.3390/cells9040812.
[49] R. L. P. van Veen, H. J. C. M. Sterenborg, A. Pifferi, A. Torricelli, E. Chikoidze, and R. Cubeddu, "Determination of visible near-IR absorption coefficients of mammalian fat using time- and spatially resolved diffuse reflectance and transmission spectroscopy," *J. Biomed. Opt.*, vol. 10, no. 5, 2005, Art. no. 054004, doi: 10.1117/1.2085149.
[50] H. Elayan, R. M. Shubair, J. M. Jornet, and P. Johari, "Terahertz channel model and link budget analysis for intrabody nanoscale communication," (in eng), *IEEE Trans. Nanobiosci.*, vol. 16, no. 6, pp. 491–503, Sep. 2017, doi: 10.1109/tnb.2017.2718967.
[51] S. O. Kasap, *Optoelectronics and Photonics*. Upper Saddle River, NJ, USA: Prentice-Hall, 2001.
[52] A. Maghoul, A. Rostami, S. Matloub, and A. Pourrezaei, "Design considerations influencing optical response in gold spherical nanoparticles," *J. Nano Res.*, vol. 46, pp. 1–11, Mar. 2017, doi: 10.4028/www.scientific.net/JNanoR.46.1.
[53] M. R. Hamblin, "Mechanisms of photobiomodulation in the brain," in *Photobiomodulation in the Brain*, M. R. Hamblin and Y.-Y. Huang, Eds. New York, NY, USA: Academic, 2019, ch. 8, pp. 97–110.
[54] N. G. A. Tan, W. Wu, and A. M. Seifalian, "Optogenetics: Lights, camera, action! A ray of light, a shadow unmasked," in *Applications of Nanoscience in Photomedicine*, M. R. Hamblin and P. Avci, Eds. Oxford, U.K.: Chandos, 2015, ch. 10, pp. 185–203.
[55] D. Lemoine, C. Habermacher, A. Martz, P.-F. Mery, N. Bouquier, F. Diverchy, A. Taly, F. Rassendren, A. Specht, and T. Grutter, "Optical control of an ion channel gate," (in eng), *Proc. Nat. Acad. Sci. USA*, vol. 110, no. 51, pp. 20813–20818, Dec. 2013, doi: 10.1073/pnas.1318715110.
[56] P. Paoletti, G. C. R. Ellis-Davies, and A. Mourot, "Optical control of neuronal ion channels and receptors," *Nature Rev. Neurosci.*, vol. 20, no. 9, pp. 514–532, Sep. 2019, doi: 10.1038/s41583-019-0197-2.
[57] M. Podbielska, N. Banik, E. Kurowska, and E. Hogan, "Myelin recovery in multiple sclerosis: The challenge of remyelination," (in eng), *Brain Sci.*, vol. 3, no. 4, pp. 1282–1324, Aug. 2013, doi: 10.3390/brainsci3031282.
[58] S. Rezaei, B. Dabirmanesh, L. Zare, A. Golestani, M. Javan, and K. Khajeh, "Enhancing myelin repair in experimental model of multiple sclerosis using immobilized chondroitinase ABC i on porous silicon nanoparticles," *Int. J. Biol. Macromolecules*, vol. 146, pp. 162–170, Mar. 2020, doi: 10.1016/j.ijbiomac.2019.12.258.
[59] K. Eom, J. Kim, J. M. Choi, T. Kang, J. W. Chang, K. M. Byun, S. B. Jun, and S. J. Kim, "Enhanced infrared neural stimulation using localized surface plasmon resonance of gold nanorods," *Small*, vol. 10, no. 19, pp. 3853–3857, Oct. 2014, doi: 10.1002/smll.201400599.
[60] S. Ojha and B. Kumar, "A review on nanotechnology based innovations in diagnosis and treatment of multiple sclerosis," *J. Cellular Immunotherapy*, vol. 4, no. 2, pp. 56–64, Dec. 2018, doi: 10.1016/j.jocit.2017.12.001.
[61] C. Paviolo and P. Stoddart, "Gold nanoparticles for modulating neuronal behavior," (in eng), *Nanomaterials*, vol. 7, no. 4, p. 92, Apr. 2017, doi: 10.3390/nano7040092.
[62] H. Zong *et al.*, "Nanoparticles carrying neurotrophin-3-modified Schwann cells promote repair of sciatic nerve defects," *Neural Regener. Res.*, vol. 8, no. 14, p. 1262, 2013.
[63] M. Polyanskiy. *Refractive Index Database*. Accessed: 2014. [Online]. Available: http://refractiveindex.info
[64] E. D. Palik, Ed., "Refractive index," in *Handbook of Optical Constants of Solids*. Burlington, VT, USA: Academic, 1997, ch. 2, pp. 5–114.

AMIR MAGHOUL received the B.S. and M.S. degrees in electrical engineering, in 2006 and 2009, respectively, and the Ph.D. degree in electrical engineering-optical integrated circuits from the University of Tabriz, Iran, in 2017.

He joined Islamic Azad University (IAU), as an Assistant Professor, in 2017. He was occupied with teaching different courses at bachelor's and master's levels. From 2017 to 2019, he continued his collaboration with the Photonic and Crystal Laboratory, University of Tabriz and ASEPE company in the nanophotonic field. He is currently pursuing his research as a Postdoctoral Fellowship with the Norwegian University of Science and Technology (NTNU), Norway. He focused on nanoantennas design, nonlinear properties of nanoantennas, and simulation of computational nanophotonic structures. His research interests include micro/nanoantenna design for optical and medical applications, computational neuroscience, and simulating in nanophotonic structures.

ALI KHALEGHI received the Ph.D. degree in physics from the University of Paris XI, Paris, France, in 2006. From 2006 to 2007, he held a postdoctoral position at the Institute d' Electronique et de Télécommunications de Rennes (IETR), France. From 2008 to 2009, he held a postdoctoral position at the Intervention Center (IVS), Oslo University Hospital, Norway. From 2010 to 2015, he was an Assistant Professor with the Electrical and Computer Engineering Department, K. N. Toosi University of Technology (KNTU), Tehran, Iran. He obtained several research and industrial grants during his career at KNTU. He established Wireless Terminal Test Lab (WTT), KNTU. He distinguished as the Best Researcher with KNTU, in 2013. Since 2015, he has been a Senior Scientist with the Norwegian University of Science and Technology (NTNU) and Oslo University Hospital. He has authored over 95 journal and full conference papers and holds five international patents. His research interests include antennas and wave propagation, wireless communications, electromagnetic compatibility (EMC), measurement techniques, and bio-electromagnetics.

ILANGKO BALASINGHAM received the M.Sc. and Ph.D. degrees in signal processing from the Department of Electronic Systems, Norwegian University of Science and Technology (NTNU), Trondheim. He is currently the Head of the Section for Medical ICT R&D and the Intervention Center, Oslo University Hospital and a Professor of medical signal processing and communications with NTNU. For the academic year 2016/2017, he was a Professor by courtesy with the Frontier Institute, Nagoya Institute of Technology, Japan. He has authored or coauthored over 270 journal and full conference papers, seven book chapters, 42 abstracts, six patents, and 20 articles in the popular press. He has given 16 invited/keynotes at international conferences. His research interests include super robust short-range communications for both in-body and on-body sensors, body area sensor networks, and nanoscale communication networks. He is a Steering Committee Member of ACM NANOCOM, an Area Editor of *Nano Communication Networks* (Elsevier), and a Specialty Chief Editor of *Frontiers in Communications and Networks*.